

ACTION: Augmentation and Computation Toolbox for Brain Network Analysis with Functional MRI

Yuqi Fang^a, Junhao Zhang^b, Linmin Wang^b, Qianqian Wang^a and Mingxia Liu^{a,*}

^aDepartment of Radiology and Biomedical Research Imaging Center, University of North Carolina at Chapel Hill, Chapel Hill, NC 27599, United States

^bSchool of Mathematics Science, Liaocheng University, Liaocheng, Shandong 252000, China

ARTICLE INFO

Keywords:

Toolbox
Functional MRI Augmentation
Brain Network Analysis
Deep Learning Model
Federated Learning

ABSTRACT

Functional magnetic resonance imaging (fMRI) has been increasingly employed to investigate functional brain activity. Many fMRI-related software/toolboxes have been developed, providing specialized algorithms for fMRI analysis. However, existing toolboxes seldom consider fMRI data augmentation, which is quite useful, especially in studies with limited or imbalanced data. Moreover, current studies usually focus on analyzing fMRI using conventional machine learning models that rely on human-engineered fMRI features, without investigating deep learning models that can automatically learn data-driven fMRI representations. In this work, we develop an open-source toolbox, called Augmentation and Computation Toolbox for brain network analysis (ACTION), offering comprehensive functions to streamline fMRI analysis. The ACTION is a Python-based and cross-platform toolbox with graphical user-friendly interfaces. It enables automatic fMRI augmentation, covering blood-oxygen-level-dependent (BOLD) signal augmentation and brain network augmentation. Many popular methods for brain network construction and network feature extraction are included. In particular, it supports constructing deep learning models, which leverage large-scale auxiliary unlabeled data (3,800+ resting-state fMRI scans) for model pretraining to enhance model performance for downstream tasks. To facilitate multi-site fMRI studies, it is also equipped with several popular federated learning strategies. Furthermore, it enables users to design and test custom algorithms through scripting, greatly improving its utility and extensibility. We demonstrate the effectiveness and user-friendliness of ACTION on real fMRI data and present the experimental results. The software, along with its source code and manual, can be accessed online.

1. Introduction

Functional magnetic resonance imaging (fMRI) provides a noninvasive imaging technique for measuring spontaneous brain activity by detecting changes in blood-oxygen-level-dependent (BOLD) signals (Fox and Raichle, 2007). It has been increasingly employed to investigate functional activities of the brain, demonstrating great clinical and practical value in many applications, including neurological disease diagnosis (Zhang et al., 2023), brain development assessment (Edde et al., 2021), and biomarker identification (Hu et al., 2021).

Currently, many fMRI-related software and toolboxes have been developed (Kruschwitz et al., 2015; Treder, 2020; Lanka et al., 2020; Waller et al., 2018; Treder, 2020; Lanka et al., 2020; Xu et al., 2018; Meunier et al., 2020; Zhou et al., 2020), offering specialized algorithms for users to facilitate fMRI analysis in an efficient and standardized manner. For example, some toolboxes (Kruschwitz et al., 2015; Zhou et al., 2020; Wang et al., 2015) focus on constructing functional connectivity networks based on fMRI and generating network topological features, which allows for identifying disease-associated brain functional alterations. Some other studies (Waller et al., 2018; Treder, 2020; Lanka et al., 2020) assist in constructing machine learning models for brain disorder analysis, which can greatly enhance the efficiency of medical decision-making.

However, existing studies usually utilize original fMRI data for computation analysis, ignoring the basic function of enhancing the size and diversity of given fMRI data (*i.e.*, data augmentation). Functional MRI augmentation is quite useful, especially in studies with limited data samples, which can help improve the robustness and generalization of the constructed learning models. Additionally, current works usually investigate fMRI using conventional machine learning models that rely on human-engineered fMRI features, without exploring deep learning models that can automatically learn data-driven fMRI feature representations. Compared with machine learning methods, deep learning models typically integrate feature learning and model construction into one united model, resulting in data-driven features, which may lead to improved prediction results.

To this end, we develop an open-source toolbox, called Augmentation and Computation Toolbox for brain network analysis (ACTION), which offers comprehensive functions to streamline fMRI analysis. The ACTION is a Python-based and cross-platform (Windows, Linux, and Mac OS) toolbox with graphical user-friendly interfaces, and its major functions can be found in Fig. 1. The ACTION features the following advantages compared to most existing works. *First*, it enables automatic fMRI data augmentation, including both BOLD signal augmentation and brain network/graph augmentation. *Second*, ACTION integrates many methods for brain functional connectivity network construction and supports extracting multiple brain network features, including node-based and graph-based features. *Third*, besides machine learning models, it also supports the

*Corresponding author

✉ mingxia_liu@med.unc.edu (M. Liu)

ORCID(s): 0000-0002-0166-0807 (M. Liu)

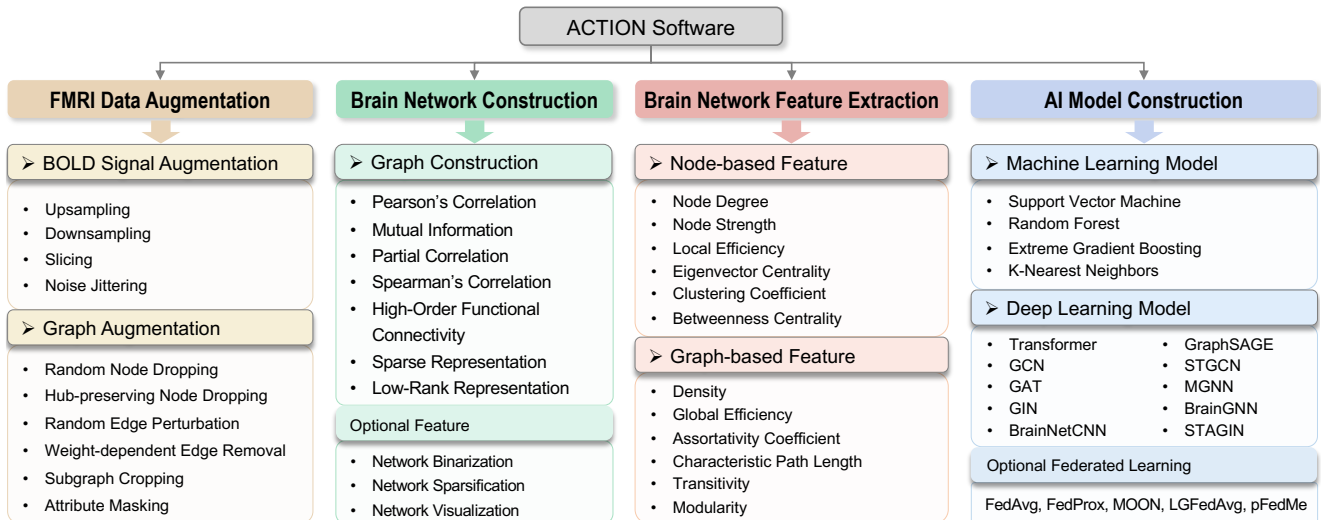


Figure 1: Major functions included in the proposed ACTION software, including fMRI data augmentation, brain network construction, brain network feature extraction, and artificial intelligence (AI) model construction.

construction of deep learning models, where ten popular methods for fMRI analysis are embedded. It is noteworthy that, for each method, our toolbox provides a pretrained deep learning model based on large-scale unlabeled fMRI data (3,800+ scans). *In addition*, it also integrates several popular federated learning strategies to facilitate multi-site fMRI studies. *Furthermore*, it enables users to design and test their custom algorithms through scripting, which greatly improves its utility and extensibility. To demonstrate the effectiveness and user-friendliness of ACTION, we employ real fMRI data for model evaluation. Detailed comparison between our ACTION and existing toolboxes for computer-aided fMRI analysis is shown in Table 1.

The remainder of this paper is organized as follows. Section 2 details the proposed ACTION, including all function modules and the corresponding algorithms. Specifically, Section 2.1 introduces two types of fMRI data augmentation. Section 2.2 and Section 2.3 present functions about brain network construction and brain network feature extraction based on fMRI data, respectively. Section 2.4 introduces artificial intelligence (AI) model construction, covering both conventional machine learning models and deep learning models. In Section 3, we validate the effectiveness of included models using real resting-state fMRI data and present the corresponding experimental results. The paper is concluded in Section 4.

2. Functions of ACTION

The ACTION software includes four major functions, *i.e.*, fMRI data augmentation, brain network construction, brain network feature extraction, and AI model construction. The software and its open-source codes can be accessed via <https://github.com/mxliu/ACTION-Software-for-Functional-MRI-Analysis/tree/main/Software>, with four function modules detailed as follows.

2.1. Functional MRI Data Augmentation

Functional MRI augmentation refers to the technique that enhances the quantity and diversity of fMRI. It usually helps improve the robustness of constructed models in fMRI analysis. Typically, there are two mainstream methods for fMRI data augmentation, *i.e.*, *BOLD signal augmentation* and *graph augmentation*. Here, a graph corresponds to a specific brain connectivity network derived from fMRI.

2.1.1. BOLD Signal Augmentation

Many fMRI studies (Li et al., 2021b; Dvornek et al., 2018; Wang et al., 2023) directly perform data augmentation based on the raw BOLD signals. These methods focus on introducing variations to fMRI time series, which simulate various temporal dynamics of brain activity. As shown in Fig. 2, four popular methods for fMRI BOLD signal augmentation are included, *i.e.*, upsampling, downsampling, slicing, and noise jittering. In addition to these methods, our toolbox also supports users to design their own BOLD signal augmentation algorithms. The details for custom algorithm deployment can be found in *Supplementary Materials*.

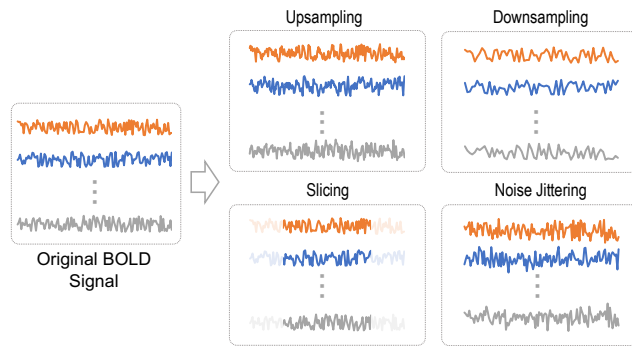
1) **Upsampling** is an augmentation strategy to stretch a time series (Le Guennec et al., 2016), which increases fMRI temporal resolution and captures more rapid neural activity changes. Specifically, given an fMRI time series with T timepoints, we perform upsampling using fast Fourier transform (Brigham, 1988) with ratio $u \in (0, 1)$. This results in a new fMRI time series with $\lfloor T/u \rfloor$ timepoints, where $\lfloor \cdot \rfloor$ represents a floor function. The newly derived data can be used for further analysis, *e.g.*, constructing brain functional networks or building learning based models.

2) **Downsampling** aims to contract a time series by decreasing its resolution (Le Guennec et al., 2016), helping capture more coarse-grained patterns and more general temporal trends. To perform downsampling, we leverage a fast Fourier transform using a ratio $b \in (0, 1)$, resulting in an fMRI time series with $\lfloor T \times b \rfloor$ timepoints.

Table 1

Comparison of major functions between the proposed ACTION and existing toolboxes for computer-aided functional MRI analysis.

Toolbox	Programming Language	Graphical User Interface	fMRI Data Augmentation	Functional Brain Network Construction	Brain Network Feature Extraction	Machine Learning Model Construction	Deep Learning Model Construction	Federated Learning for Multi-site fMRI Analysis
PyMVPA (Hanke et al., 2009)	Python	×	×	×	×	✓ (Classification, Regression)	×	×
BCT (Rubinov and Sporns, 2010)	Matlab	×	×	×	✓	×	×	×
REST (Song et al., 2011)	Matlab	✓	×	✓	×	×	×	×
CONN (Whitfield-Gabrieli et al., 2012)	Matlab	✓	×	✓	✓	×	×	×
PRoNTo (Schrouff et al., 2013)	Matlab	✓	×	×	×	✓ (Classification, Regression)	×	×
MANIA (Grotegerd et al., 2014)	Matlab	✓	×	×	×	✓ (Classification)	×	×
DynamicBC (Liao et al., 2014)	Matlab	✓	×	✓	✓	×	×	×
BASCO (Göttlich et al., 2015)	Matlab	✓	×	✓	✓	×	×	×
GraphVar (Kruschwitz et al., 2015)	Matlab	✓	×	✓	✓	×	×	×
GRETNA (Wang et al., 2015)	Matlab	✓	×	✓	✓	×	×	×
GraphVar 2.0 (Waller et al., 2018)	Matlab	✓	×	✓	✓	✓ (Classification, Regression)	×	×
BRANT (Xu et al., 2018)	Matlab	✓	×	✓	✓	×	×	×
MVPA-Light (Treder, 2020)	Matlab	×	×	×	×	✓ (Classification, Regression)	×	×
BrainNetClass (Zhou et al., 2020)	Matlab	✓	×	✓	✓	✓ (Classification)	×	×
MALINI (Lanka et al., 2020)	Matlab	✓	×	✓	×	✓ (Classification, Regression)	×	×
NeuroPycon (Meunier et al., 2020)	Python	×	×	✓	✓	×	×	×
ACTION (Ours)	Python	✓	✓	✓	✓	✓ (Classification, Regression)	✓	✓

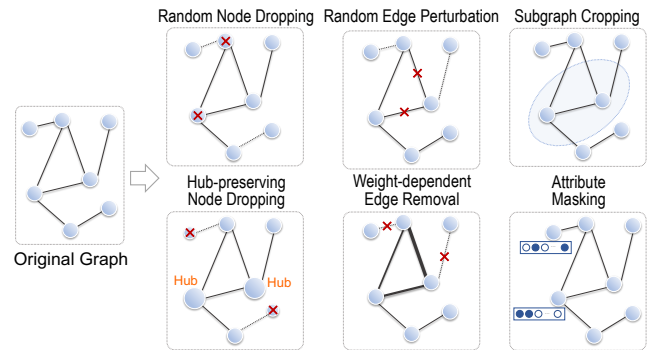
**Figure 2:** Illustration of four methods for fMRI blood-oxygen-level-dependent (BOLD) signal augmentation.

3) **Slicing** focuses on dividing the fMRI time series data into smaller segments (Le Guennec et al., 2016). Each segment represents a subset of the original time series, which captures localized temporal patterns of fMRI data. Given an fMRI with T timepoints and a slicing ratio $s \in (0, 1)$, we can derive a segmented fMRI with length $\lfloor T \times s \rfloor$, and the starting point of the new time series can change dynamically.

4) **Noise Jittering** (Wen et al., 2021) is to add random noise to the fMRI data, simulating real-world noise such as motion artifacts. Here, we employ Gaussian noise to introduce randomness to fMRI time series. Gaussian noise is a type of noise with the probability density function following the normal distribution. We denote Gaussian noise as $g \in \mathbb{R}^T$. Each element of g is a sample from the normal distribution $N(\mu, \sigma)$, where μ and σ denote the expectation/mean and standard deviation of the distribution. Given an fMRI time series $X \in \mathbb{R}^T$ and noise g , we can easily generate the new time series: $X + g$.

2.1.2. Graph Augmentation

Rather than directly manipulate original fMRI time series for data augmentation, some other fMRI studies (Pei et al., 2022) focus on first representing the brain as a functional connectivity network and then augmenting the

**Figure 3:** Illustration of six graph augmentation methods based on fMRI-derived brain networks/graphs.

brain network to increase data diversity. Each brain network contains a set of interconnected brain regions that exhibit correlated or synchronized functional activity patterns. These networks are often represented as *graphs*, where graph nodes denote brain regions-of-interest (ROIs) and graph edges mean functional connections between paired ROIs. Graph augmentation aims to introduce variability to the brain network/graphs constructed by fMRI, such as dropping nodes, perturbing edges, or modifying graph structure. With graph augmentation, we can capture a wider range of potential functional connectivity patterns of the brain, helping facilitate fMRI data analysis and advance our understanding of brain functionality.

Denote a brain network/graph as $G = \{V, E, A\}$, where each node $v_i \in V$ represents a brain ROI with its feature vector $h_i \in \mathbb{R}^D$, and E denotes the edge set. $A \in \mathbb{R}^{N \times N}$ is a matrix with each element a_{ij} denoting functional connectivity between the i -th and the j -th ROIs, where N denotes the number of nodes/ROIs. In ACTION, we introduce six methods for graph augmentation (see Fig. 3), including four popular methods (*i.e.*, random node dropping, random edge perturbation, subgraph cropping, and attribute masking) and two recently designed methods (*i.e.*, hub-preserving node dropping and weight-dependent edge removal).

1) **Random Node Dropping** (You et al., 2020) aims to randomly remove a certain proportion of graph nodes along with their associated edges from G . The probability of dropping each node follows a uniform distribution, and the node dropping rate σ ranges from 0 to 1. For instance, if σ is set as 0.05, it means that 5% of graph nodes, along with the connected edges, are randomly discarded.

2) **Hub-Preserving Node Dropping** is a recently designed algorithm for graph augmentation, which prioritizes preserving brain hub regions during this procedure. Brain hubs refer to brain regions that exhibit a high degree of functional connectivity with other regions and they usually play a significant role in facilitating effective interaction within the brain. Here, we employ degree centrality (Rubinov and Sporns, 2010) to measure the importance of each node and determine the dropping probability based on its degree centrality d_i . Specifically, the probability of the node v_i being dropped is represented as $q_i = 1/d_i$. In this way, the nodes with a higher degree centrality exhibit a lower dropping probability. Then, we obtain probability distribution p_i for node v_i based on normalization: $p_i = q_i / \sum_{i=1} q_i$. Following this probability distribution, we drop certain nodes according to a specified drop ratio $c \in (0, 1)$ for graph augmentation.

3) **Random Edge Perturbation** (You et al., 2020) aims to perturb the graph edges in G by randomly adding or dropping a certain proportion of edges, while maintaining the total number of edges consistent with the original graph. The probability of adding or dropping each edge follows a uniform distribution, with an edge adding/dropping ratio $e \in (0, 1)$. If e is set as 0.1, 10% edges are randomly removed, and 10% edges are randomly added.

4) **Weight-Dependent Edge Removal** is a graph augmentation method based on edge perturbation. Rather than randomly remove edges, it performs edge dropping by considering edge importance/weight (*i.e.*, a_{ij}). Specifically, it uses Pearson's correlation coefficient (Freedman et al., 2007) to measure the edge weight a_{ij} , and the probability for an edge e_{ij} being removed is defined as $p_{ij} = q_{ij} / \sum_{i=1} \sum_{j=1} q_{ij}$, where $q_{ij} = 1/a_{ij}$. That is, the edges with stronger functional connectivity have a lower probability of being dropped. According to this probability, we remove a certain proportion of edges to generate augmented graphs based on a given dropping ratio.

5) **Subgraph Cropping** (You et al., 2020) randomly selects a subset of brain regions and their associated functional connections to create a smaller subnetwork based on a random walk. The underlying assumption is that the semantic information of G can be well preserved within its partial graph structure.

6) **Attribute Masking** (You et al., 2020) involves randomly masking attributes or features associated with certain brain regions/nodes. It assumes that missing partial node features do not impact the whole graph much.

In addition to the above-mentioned methods, users can design and use their custom graph augmentation algorithms.

More details on implementing self-defined graph augmentation algorithms can be found in *Supplementary Materials*.

2.2. Brain Network Construction

Our toolbox includes seven popular methods for brain network construction, *i.e.*, *Pearson's correlation*, *mutual information*, *partial correlation*, *Spearman's correlation*, *high-order functional connectivity*, *sparse representation*, and *low-rank representation*. It also embeds two network sparsification strategies, helping focus on the strong connections representing neural processes. Moreover, it supports brain network visualization, allowing users to identify functional connectivity patterns that may not be apparent shown in original data. The algorithms for network construction and the details of network sparsification and visualization are detailed as follows.

2.2.1. Network Construction Methods

1) **Pearson's Correlation (PC)** (Cohen et al., 2009) measures linear relationships between fMRI time series of different brain regions. Denote X and Y as fMRI time series of two brain regions, and the PC coefficient between X and Y can be derived using:

$$PC_{XY} = \frac{cov(X, Y)}{\sigma_X \sigma_Y}, \quad (1)$$

where $cov(X, Y)$ denotes the covariance between X and Y , and σ_X and σ_Y represent the standard deviation of X and Y , respectively. Typically, PC_{XY} ranges from -1 and 1 . A value close to 1 indicates stronger positive synchronization between X and Y , suggesting that the corresponding brain regions are functionally connected and likely involved in similar neural processes. And a value close to -1 indicates a strong negative relationship. A value close to 0 suggests no linear relationship between time series of paired regions.

2) **Mutual Information (MI)** (Kraskov et al., 2004) quantifies the amount of information we can obtain from one fMRI time series by observing the other fMRI time series. Mathematically, the MI between two fMRI time series X and Y can be represented as:

$$MI_{XY} = \sum_{y \in Y} \sum_{x \in X} p(x, y) \log \left(\frac{p(x, y)}{p(x)p(y)} \right), \quad (2)$$

where $p(x, y)$ denotes the joint probability distribution function of X and Y . And $p(x)$ and $p(y)$ are the marginal probability distribution functions of X and Y , respectively. A higher value of MI_{XY} indicates a stronger dependency between two fMRI time series, indicating greater synchronization in neural activity between two brain regions. If MI_{XY} is close to 0 , it suggests that two fMRI time series are independent. Compared with Pearson's correlation, which only measures the linear relationship between two time series, mutual information can capture both linear and nonlinear relationships between them.

3) **Partial Correlation (PrC)** (De La Fuente et al., 2004) examines the relationship between fMRI time series of two

regions while controlling for the influence of other brain regions. The partial correlation coefficient between two fMRI time series X and Y can be denoted as follows:

$$PrC_{XY} = \frac{\rho_{XY} - \rho_{XZ}\rho_{YZ}}{\sqrt{(1 - \rho_{XZ}^2)(1 - \rho_{YZ}^2)}}, \quad (3)$$

where Z represents the time series of all the other remaining regions. $\rho_{XY} = cov(X, Y)/\sigma_X\sigma_Y$, $\rho_{XZ} = cov(X, Z)/\sigma_X\sigma_Z$, and $\rho_{YZ} = cov(Y, Z)/\sigma_Y\sigma_Z$. Like the Pearson's correlation coefficient, PrC_{XY} also ranges from -1 and 1 . A higher value indicates a stronger linear relationship between the two fMRI time series after removing the effect of the other regions. If the value of PrC_{XY} is 0 , it indicates no linear relationship between the two time series.

4) **Spearman's Correlation (SC)** (Xiao et al., 2016) quantifies the strength of the monotonic relationship between two fMRI time series. To obtain SC coefficient between two time series X and Y , X and Y are first converted to ranked values, followed by:

$$SC_{XY} = 1 - \frac{6 \sum d_t^2}{T(T^2 - 1)}, \quad (4)$$

where d_t is the difference between the ranks of X and Y , represented as $d_t = Rank_X(t) - Rank_Y(t)$, and T is the number of timepoints. SC_{XY} also ranges from -1 and 1 , where a value of -1 or 1 implies an exact monotonic relationship between X and Y , while a value of 0 indicates no correlation.

5) **High-Order Functional Connectivity (HOFC)** (Zhang et al., 2016) is a measure to examine high-level organization of brain functionality. Unlike traditional low-order networks (*e.g.*, constructed by Pearson's correlation) that often use functional correlation measures between any pair of brain regions, a HOFC network is constructed based on "correlation's correlation", helping characterize high-level inter-region interactions. Specifically, given the low-order brain network $P \in \mathbb{R}^{N \times N}$, which is constructed based on Pearson's correlation, HOFC between the i -th and j -th regions can be formulated as:

$$HOFC_{ij} = \frac{\sum_k (P_{ik} - \bar{P}_i)(P_{jk} - \bar{P}_j)}{\sqrt{\sum_k (P_{ik} - \bar{P}_i)^2} \sqrt{\sum_k (P_{jk} - \bar{P}_j)^2}}, \quad (5)$$

where a higher value of $HOFC_{ij}$ represents a stronger high-order relationship between the two regions.

6) **Sparse Representation (SR)** (Xu et al., 2012) estimates sparse brain functional networks by introducing an $L1$ -regularizer, which can effectively filter out weak or redundant connections in the network. Mathematically, the objective function for SR-based brain network estimation can be represented as:

$$\min_W \|X - XW\|_2^2 + \lambda \|W\|_1, \quad (6)$$

where $W \in \mathbb{R}^{N \times N}$ is expect to represent the original fMRI data X in a sparse manner. λ is the regularization

parameter controlling the sparsity level, and a larger value helps produce a sparser brain network.

7) **Low-rank Representation (LR)** (Recht et al., 2010) helps construct brain networks in a low-rank learning manner. Specifically, its optimization is formulated as:

$$\min_W \|X - XW\|_2^2 + \lambda \|W\|_*, \quad (7)$$

where $W \in \mathbb{R}^{N \times N}$ is expected to well represent the original fMRI data X and has a low-rank structure. $\|W\|_*$ denotes the trace norm (*i.e.*, nuclear norm) of W , which is the sum of the singular values of W . λ is a regularization parameter, with a higher value encouraging a lower-rank brain network. The low-rank network can represent the original network with fewer components, helping identify the most significant connections and filter out less relevant connections.

It is noted that, besides these methods, users are allowed to use their self-defined algorithms for brain network construction based on fMRI data. The specific details are elaborated in the *Supplementary Materials*.

2.2.2. Brain Network Sparsification

Our toolbox offers two sparsification strategies, allowing users to sparsify the constructed brain networks:

1) **Sparsity**. This method retains the top $K\%$ values of constructed brain networks while setting the rest to 0 . In our toolbox, the K is set to 30 by default. Compared with the fully connected brain network, the network constructed using "Sparsity" can preserve strong connections while removing the weak ones.

2) **Binarization**. This method follows the same strategy as used in "Sparsity", but converts all weighted connections to binary ones.

2.2.3. Brain Network Visualization

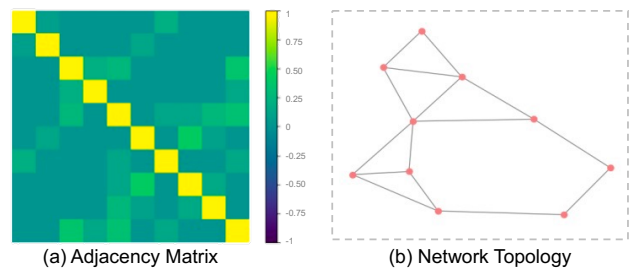


Figure 4: Visualization of the constructed brain network.

As a useful addition, this toolbox allows the users to visualize the constructed brain networks from two perspectives, *i.e.*, *adjacency matrix* and *network topology*.

1) **Adjacency Matrix**. The constructed brain network can be represented as the adjacency matrix, where each row and column corresponds to a different brain region, and each entry denotes the functional connections between regions. Here, we use a simulated time series $X \in \mathbb{R}^{N \times T}$ to construct a brain network based on Pearson's correlation, where $N = 10$ and $T = 30$ denote the numbers of regions and timepoints,

respectively. We retain the top 50% functional connections by setting the Sparsity ratio K to 50. The illustration of the adjacency matrix is shown in Fig. 4 (a).

2) **Network Topology**. As seen in Fig. 4 (b), we also show the network topology of the constructed brain network based on the same simulated time series. Here, each graph node represents each brain region, and each graph edge denotes the functional connection between regions.

2.3. Brain Network Feature Extraction

Based on the constructed brain networks/graphs, we can extract various network features for further fMRI analysis, which are essential for understanding brain functional connectivity patterns. Typically, there are two main types of brain network features, *i.e.*, node-based features and graph-based features. The node-based features are computed for each graph node (*i.e.*, brain region), helping investigate the importance of individual brain regions within the brain network. The graph-based features capture global network properties and characterize interactions across brain regions, which provide a holistic view of the entire brain network. It is noted that our toolbox supports selecting multiple network features simultaneously.

2.3.1. Node-based Brain Network Features

Denote functional relationship between v_i and v_j as $a_{ij} \in \mathbb{R}^{N \times N}$, where a_{ij} can be binary or weighted. When a_{ij} is binary, $a_{ij}=1$ if v_i and v_j connect with each other, otherwise $a_{ij}=0$. When a_{ij} is weighted, a_{ij} represents the functional connectivities between v_i and v_j . In our work, we introduce six node-based network features, including *node degree*, *node strength*, *local efficiency*, *betweenness centrality*, *eigenvector centrality*, and *clustering coefficient*.

1) **Node Degree (ND)** (Zegura et al., 1996) calculates the number of edges connected to a node or brain ROI. Mathematically, the node degree of v_i can be formulated as:

$$ND_i = \sum_{j \in N} \mathbf{1}(a_{ij} \neq 0). \quad (8)$$

The brain region with a higher degree represents that it is functionally connected to a greater number of other regions, indicating that it may play a significant role in information communication within the brain network.

2) **Node Strength (NS)** (Barrat et al., 2004) measures a weighted variant of the degree, which is defined as the sum of all neighboring edge weights:

$$NS_i = \sum_{j \in N} a_{ij}. \quad (9)$$

Node strength is particularly useful in representing brain networks when the connections between brain regions are weighted. NS_i represents the accumulated functional connectivity between node v_i and the remaining ones. If a_{ij} is binary, NS_i is similar to ND_i .

3) **Local Efficiency (LE)** (Latora and Marchiori, 2001) is a measure that quantifies how well a specific brain region

communicates with its immediate neighbors, defined as:

$$LE = \frac{1}{n} \sum_{i \in V} \frac{\sum_{j, h \in V, j \neq i} a_{ij} a_{ih} [d_{jh}(N_i)]^{-1}}{k_i (k_i - 1)}, \quad (10)$$

where $d_{jh}(N_i)$ is the shortest path length between v_j and v_h that involves only neighboring regions of v_i , and k_i is degree of node v_i . A brain region with higher local efficiency indicates that it communicates with its neighbors efficiently. And a brain network with more such kinds of regions tends to form more densely interconnected clusters, which may facilitate rapid information exchange within the network.

4) **Betweenness Centrality (BC)** (Freeman et al., 2002) is an important measure in functional brain network analysis. Given a node v_i , its betweenness centrality is calculated as the fraction of shortest paths between all pairs of regions in the network that pass through v_i , defined as:

$$BC_i = \frac{1}{(N-1)(N-2)} \sum_{h, j \in V, h \neq j, j \neq i, i \neq h} \frac{\rho_{hj}(i)}{\rho_{hj}}, \quad (11)$$

where ρ_{hj} denotes the number of shortest paths between v_h and v_j , and $\rho_{hj}(i)$ represents the number of shortest paths between v_h and v_j that pass through v_i . A brain region with a higher BC mean indicates it serves as a critical hub connecting different parts of the network, suggesting that it plays an important role in information transfer within the brain network.

5) **Eigenvector Centrality (EC)** (Bonacich, 2007) quantifies the influence of a brain region based on its connections to other important regions. Mathematically, the EC of a node v_i is calculated as the eigenvector corresponding to the largest eigenvalue of the adjacency matrix (*i.e.*, A) of the network, represented as:

$$EC_i = \frac{1}{\lambda} \sum_{j \in V} A_{ij} EC_j, \quad (12)$$

where λ is the largest eigenvalue of A , and EC_j represents the eigenvector centrality of node v_j . A brain region will have a high EC if it is strongly connected with other regions that play significant roles within the network, and thus, EC helps identify influential hub regions in functional networks.

6) **Clustering Coefficient (CC)** (Watts and Strogatz, 1998) represents the abundance of connected triangles in a brain network. Given a brain region v_i , its CC is computed as the fraction of triangles that exist among the neighbors of v_i out of the all possible number of triangles that could exist among them, defined as follows:

$$CC_i = \frac{1}{n} \sum_{i \in V} \frac{2t_i}{k_i (k_i - 1)}, \quad (13)$$

where $t_i = \frac{1}{2} \sum_{j, h \in V} a_{ij} a_{ih} a_{jh}$ denotes the number of triangles around a node v_i , and k_i is degree of node v_i . A node with higher CC indicates that its neighboring regions tend to form tighter interconnected clusters.

2.3.2. Graph-based Brain Network Features

We also introduce six graph-based network features, including *density*, *modularity*, *characteristic path length*, *global efficiency*, *assortativity coefficient*, and *transitivity*.

1) **Density** (Kaiser, 2011) quantifies the level of connectivity in the network to measure the percentage of existing connections among all possible connections, defined as:

$$D = \frac{2l}{N(N-1)}, \quad (14)$$

where l denotes the number of edges in a brain network. A brain network with higher density suggests that the brain regions are connected more densely.

2) **Modularity** (Newman, 2006) quantifies the extent to which a network can be partitioned into non-overlapping and functionally distinct subnetworks, defined as:

$$M = \frac{1}{2l} \sum_{i,j \in V} \left(a_{ij} - \frac{k_i k_j}{2l} \right) \delta_{m_i, m_j}, \quad (15)$$

where m_i is the module containing node i , and δ_{m_i, m_j} equals 1 if v_i and v_j belong to the same module, otherwise it is 0. k_i denotes degree of node v_i and l represents the number of edges. A brain network with high modularity indicates that it has a modular structure, and brain regions within the same module may share similar functional roles.

3) **Characteristic Path Length (CPL)** (Watts and Strogatz, 1998) measures the average shortest path length (distance) between all pairs of nodes in the brain network, which can be formulated as:

$$CPL = \frac{1}{N} \sum_{i \in V} \frac{\sum_{j \in V, j \neq i} d_{ij}}{N-1}, \quad (16)$$

where d_{ij} is the shortest path between v_i and v_j . A brain network with higher CPL indicates that information takes longer to transfer across different brain regions, implying lower communication efficiency. This measure is the most commonly used metric in functional brain network analysis, and many studies have found that its alteration is highly correlated with brain disease disorders, such as Alzheimer's disease (Dai et al., 2019), Parkinson's disease (Ma et al., 2017), and epilepsy (Paldino et al., 2017).

4) **Global Efficiency (GE)** (Latora and Marchiori, 2001) quantifies the efficiency of information transfer across brain regions in the entire network. It is defined as the average of the inverse of the shortest path lengths between all pairs of nodes, represented as:

$$GE = \frac{1}{N} \sum_{i \in V} \frac{\sum_{j \in V, j \neq i} d_{ij}^{-1}}{N-1}, \quad (17)$$

where d_{ij} denotes the shortest path between v_i and v_j . A higher global efficiency indicates shorter average path lengths between nodes, suggesting more efficient information transmission across different brain regions.

5) **Assortativity Coefficient (AC)** (Newman, 2002) quantifies the tendency of nodes with similar degree patterns

to connect, which is denoted as:

$$AC = \frac{l^{-1} \sum_{(i,j) \in E} k_i k_j - \left[l^{-1} \sum_{(i,j) \in E} \frac{1}{2} (k_i + k_j) \right]^2}{l^{-1} \sum_{(i,j) \in E} \frac{1}{2} (k_i^2 + k_j^2) - \left[l^{-1} \sum_{(i,j) \in E} \frac{1}{2} (k_i + k_j) \right]^2}, \quad (18)$$

where k_i is degree of node v_i , E is the edge set, and l is the number of edges. AC can provide insights into the organization of connections within the brain network. A network with larger AC denotes that brain regions tend to connect with other regions of similar degree. For instance, regions with high degrees are more likely to associate with other high-degree regions, which may identify the brain hubs. Conversely, a brain network with smaller AC suggests that high-degree regions tend to connect with low-degree regions, which implies a more distributed network topology.

6) **Transitivity** (Newman, 2003) is a measure that quantifies the extent to which connections between neighboring regions are likely to form clusters (e.g., triangles) within the network, which is represented as:

$$T = \frac{\sum_{i \in V} 2t_i}{\sum_{i \in V} k_i (k_i - 1)}, \quad (19)$$

where $t_i = \frac{1}{2} \sum_{j,h \in V} a_{ij} a_{ih} a_{jh}$ denotes the number of triangles around a node v_i . k_i is degree of node v_i . A higher transitivity indicates that neighboring brain regions are more interconnected, forming local clusters in the network.

2.4. Artificial Intelligence Model Construction

There is an emerging trend to leverage fMRI data to construct artificial intelligence models for prediction, such as disease diagnosis (Fang et al., 2023), age estimation (Lund et al., 2022), brain state detection (Wang et al., 2018). Many existing toolboxes (Lanka et al., 2020; Zhou et al., 2020; Treder, 2020; Waller et al., 2018) have investigated conventional machine learning models for analyzing fMRI, which mainly rely on hand-crafted features for model construction. Besides including these conventional models, our toolbox also embeds popular deep learning models for prediction, which are neglected by previous studies. The deep learning models can learn data-driven fMRI features guided by downstream tasks, eliminating the need for domain expertise to manually design features. It is noted that we incorporate a pretraining strategy into each deep learning model, resulting in a backbone encoder with high generalizability that can adapt well to a new dataset/task. Moreover, we integrate federated learning strategies for each deep learning model, allowing it to be trained using multiple data sites collaboratively while keeping the data decentralized and private.

2.4.1. Conventional Machine Learning Models

Typically, the conventional machine learning models take human-engineered fMRI features as input and then perform model prediction. In our toolbox, users can construct machine learning models for both classification and regression tasks, and the whole framework is illustrated in Fig. 5. Specifically, given the input fMRI features, we can

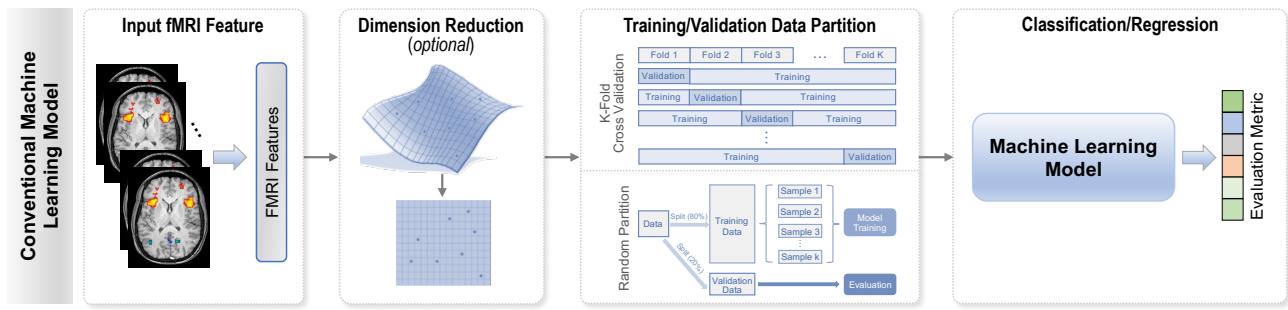


Figure 5: Illustration of conventional machine learning framework for fMRI-based prediction.

first reduce the feature dimensions, which may eliminate noise and irrelevant features, helping reduce the overfitting issue. Based on the derived features, we can construct machine learning models for classification/regression. Several evaluation metrics are provided to verify the effectiveness of the constructed models. By integrating feature dimension reduction, model construction, and model evaluation into a united framework, our toolbox enables streamlined model prediction based on fMRI features. The main components in this machine learning framework are detailed as follows.

Techniques for Feature Dimension Reduction. Since the input fMRI features may be high-dimensional, our toolbox allows users to reduce feature dimensions before performing classification/regression. Three popular dimension reduction techniques are embedded in ACTION, including:

- Principal Component Analysis (PCA) (Wold et al., 1987), which reduces dimension by keeping the features (*i.e.*, principal components) that contribute most to data variance;
- Independent Component Analysis (ICA) (Hyvärinen and Oja, 1997), which performs dimension reduction by separating the features into a set of additive and independent non-Gaussian components;
- Canonical Correlation Analysis (CCA) (Hotelling, 1992), which aims to extract the most informative dimensions by identifying linear combinations that maximize the correlation of the input features.

Model Description. This toolbox integrates several popular machine learning models to analyze fMRI, including:

- Support Vector Machine (SVM) (Hearst et al., 1998), which performs prediction by finding the hyperplane that best separates different classes of data with maximum margin;
- Random Forest (RF) (Breiman, 2001), which is an ensemble learning method that builds multiple decision trees and merges them to obtain prediction;
- Extreme Gradient Boosting (XGBoost) (Chen and Guestrin, 2016), which is an optimized ensemble learning method that combines decision trees and gradient boosting for prediction;

- K-Nearest Neighbors (KNN) (Fix, 1985), which performs prediction based on the majority class or average of its nearest neighbors in the feature space.

These methods are suited for classification and regression tasks, enabling users to address different downstream tasks. Users can design and use their self-defined models for classification/regression, with details given in *Supplementary Materials*. Users can utilize fMRI features derived from ACTION (*e.g.*, “brain network feature extraction” module), and also take features generated by themselves.

Data Partition Strategies. We divide the input data into training and validation sets to evaluate the performance of the machine learning models. The training set is used to train the model while the validation set is used to assess model performance based on the trained model. Our toolbox provides two different data partition strategies:

- *K*-fold Cross Validation: This strategy divides the input data into *K* distinct subsets. During model training, one subset is treated as the validation set to evaluate model performance, while the remaining *K*-1 subsets are used for model training. This process is repeated *K* times, with each *K* subset serving as the validation set once. The final prediction is derived by averaging the results from these *K*-fold validation results. This data partition strategy ensures the model is validated across all samples.
- Random Partition: This strategy randomly divides the input data according to a specified partition ratio *R*%. That is, *R*% data samples are used for model training while the remaining data are used for validation.

Evaluation Metrics. Our toolbox provides several metrics for model evaluation. For classification tasks, seven metrics are used: area under the receiver operating characteristic curve (AUC), accuracy, balanced accuracy, F1-score, sensitivity, specificity, and precision. It also allows users to plot confusion matrices and AUC to visualize classification results. For regression tasks, we evaluate the model using mean absolute error, mean squared error, and concordance correlation coefficient in this toolbox.

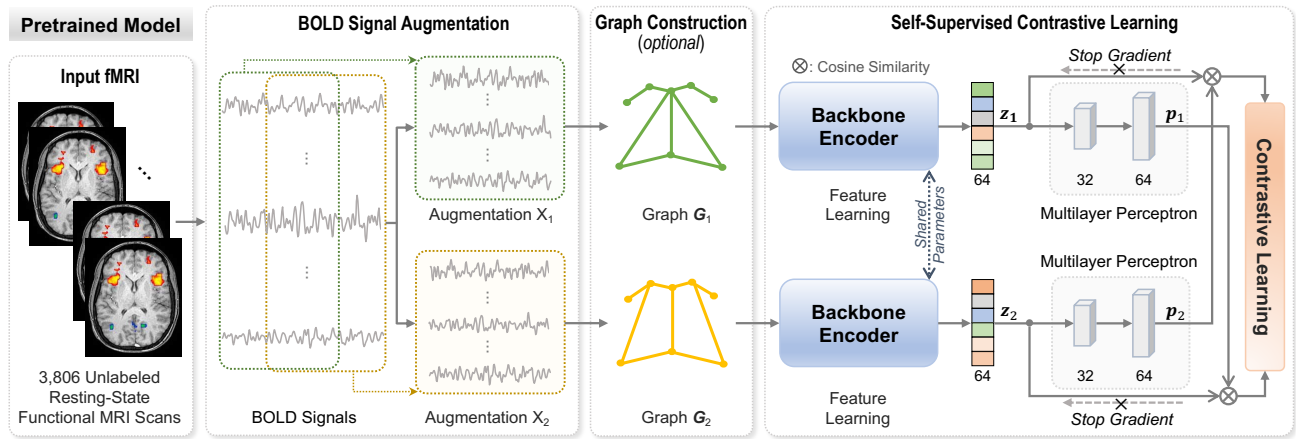


Figure 6: Illustration of self-supervised contrastive learning framework for pretraining deep learning models with fMRI.

2.4.2. Deep Learning Models

In ACTION, we incorporate ten popular deep learning methods for computer-aided fMRI analysis. Moreover, for each method, our toolbox constructs a pretrained deep learning model based on large-scale unlabeled fMRI data in a self-supervised manner. As the pretrained models are built based on large and diverse fMRI data, they are expected to capture more general fMRI features, helping improve model performance in downstream tasks. In addition, the pretrained models can be used to finetune downstream tasks with limited sample sizes, facilitating effective knowledge transfer and reducing the model overfitting issue.

The framework for constructing a pretrained deep learning model is illustrated in Fig. 6. For training the model, we use 3,806 resting-state fMRI scans from three public datasets, including Autism Brain Imaging Data Exchange (ABIDE) initiative¹, REST-meta-MDD Consortium², and ADHD-200³. The selection criteria of these fMRI scans and their ID information are given in *Supplementary Materials*. As shown in Fig. 6, the framework contains three main components, including fMRI BOLD signal augmentation, graph construction, and self-supervised contrastive learning. With 3,806 fMRI time series as input, we first perform data augmentation using a slicing strategy, yielding two augmented signals X_1 and X_2 . Here, X_1 and X_2 are obtained by segmenting the first 90% and the last 90% of full-length signals, respectively. Then, they are fed into a graph construction module for fMRI feature learning. This step is optional, depending on the specific architecture of deep learning methods. After that, X_i or $G(X_i)$ ($i=1$ or 2) are input to two shared backbone encoders for feature learning, resulting in fMRI representations z_1 and z_2 , respectively. Based on z_1 and z_2 , we leverage two multilayer perceptron (MLP) layers to abstract higher-level feature representations p_1 and p_2 . Inspired by SimSiam (Chen and He, 2021), the pretrained model is optimized by maximizing the agreement between two augmented features based on contrastive learning. The

main idea is to enforce the consistency of augmented features from the same fMRI scan. Mathematically, this optimization process is as follows:

$$\mathcal{L}_C = \Phi(\psi(z_1), p_2) + \Phi(\psi(z_2), p_1), \quad (20)$$

where Φ denotes the negative cosine similarity and ψ represents the stop-gradient operation, which enables the stability of the training process (Chen and He, 2021). After obtaining the pretrained backbone encoder, we can finetune it based on users' downstream tasks, helping adapt the model to a new fMRI dataset. The specific finetuning process for each deep learning method is detailed in our open-source code.

In the following, we detail the ten deep learning methods included in ACTION for fMRI analysis.

1) Transformer (Vaswani et al., 2017), a deep learning model based on self-attention, has become foundational for processing sequential data. For fMRI analysis, we first construct the brain network based on fMRI time series via Pearson's correlation. We then leverage self-attention to dynamically weigh the importance of different regions in the network, capturing dependencies among brain regions.

2) Graph Convolutional Network (GCN) (Kipf and Welling, 2016) is a powerful graph neural network designed specifically for handling graph-structured data, e.g., brain networks. In our case, we also use Pearson's correlation to construct the brain network/graph. Then, we utilize two stacked graph convolutional layers to update and aggregate the representations of each graph node/brain region, yielding a hierarchical representation of the brain network.

3) Graph Attention Network (GAT) (Velivcković et al., 2017) extends the concept of GCN (Kipf and Welling, 2016) by introducing the mechanism of attention. Unlike GCN which treats contributions of all regions equally, GAT employs a learnable attention mask that dynamically assigns different weights to each brain region, enabling the model to focus more on task-relevant information.

4) Graph Isomorphism Network (GIN) (Kim and Ye, 2020) achieves maximum discriminative power among graph neural networks by generalizing the Weisfeiler-Lehman (WL) test. Like GCN (Kipf and Welling, 2016),

¹http://fcon_1000.projects.nitrc.org/indi/abide

²<http://rfmri.org/REST-meta-MDD>

³http://fcon_1000.projects.nitrc.org/indi/adhd200/

with the brain network as input, we stack two GIN layers for fMRI feature learning, followed by a pooling operation to generate a graph representation.

5) Graph Sample and Aggregate (GraphSAGE) (Hamilton et al., 2017) is a method designed for analyzing graph-structured data. With the brain network as input, GraphSAGE learns node representations by sampling and aggregating information from its local neighborhood. To abstract fMRI features, two GraphSAGE layers are leveraged, followed by a pooling operation.

6) Brain Network Convolutional Neural Network (BrainNetCNN) (Kawahara et al., 2017) is specially designed for brain network analysis, consisting of 3 convolutional filters (edge-to-edge, edge-to-node, and node-to-graph) to capture topological structure information of brain networks.

7) Brain Graph Neural Network (BrainGNN) (Li et al., 2021b) is a graph neural network designed for analyzing fMRI and detecting neurological biomarkers. With the brain network as input, BrainGNN uses two node-level graph convolutional layers to learn the node representations, capturing topological and functional patterns from fMRI data.

8) Spatio-Temporal Graph Convolutional Network (STGCN) (Gadgil et al., 2020) is designed to jointly extract spatial and temporal features from fMRI times series via spatiotemporal graph convolution units (GCUs). Here, we stack two GCUs to model spatiotemporal patterns, and then generate a graph representation via a pooling operation.

9) Spatio-Temporal Attention Graph Isomorphism Network (STAGIN) (Kim et al., 2021) is designed to model fMRI dynamics using spatiotemporal attention. Specifically, it first partitions the fMRI time series using a sliding-window scheme and employs GIN (Kim and Ye, 2020) to aggregate node features in each window. Then, a Transformer (Vaswani et al., 2017) is leveraged to capture temporal attention across different windows to characterize fMRI dynamics, resulting in a spatiotemporal graph representation.

10) Modularity-constrained Graph Neural Network (MGNN) (Wang et al., 2024) is specially designed to learn spatiotemporal dynamic representations of fMRI. MGNN provides a novel scheme to incorporate brain modularity to learn fMRI features, which encourages node representations within the same module to be similar. A graph-level feature representation is then generated via a pooling operation.

Additionally, our toolbox offers five federated learning strategies, which allow the model to be trained across many decentralized data sites, facilitating multi-site fMRI studies. These strategies are introduced in the following.

1) Federated Averaging (**FedAvg**) (McMahan et al., 2017) is a widely-used distributed learning paradigm. Specifically, the local sites first copy the global model parameters, which are initialized randomly or by our pretrained model. These sites independently calculate gradients based on their local data and send the gradients' updates to the central server. The server then updates the global model by averaging these updates, and the updated model is sent back to each site for the next training round.

2) Federated Proximal (**FedProx**) (Li et al., 2020), which refines FedAvg by addressing cross-site heterogeneity. Specifically, like FedAvg, FedProx first obtains a global model by averaging parameters received from each local site. Then, it mitigates the bias between global and local model parameters by introducing a regularization (*i.e.*, proximal term) to the optimization objective for each site, helping eliminate parameter drift.

3) Model-Contrastive Federated Learning (**MOON**) (Li et al., 2021a), which is designed based on FedAvg, where a global model is first constructed by averaging local sites' parameters. Then, it maximizes the similarity between representations learned by the local and global models, and minimizes the similarity between representations of the local model in the current training round and that in the previous round, helping correct the local training.

4) Local Global Federated Averaging (**LGFedAvg**) (Liang et al., 2020), which captures compact local representations on each site and a global model across all sites. Specifically, it sends the parameters of the last layer in the local site to the central server for aggregation while other parameters remain at each local site. In this way, the number of communication parameters can be much smaller than other federated learning algorithms, *e.g.*, FedAvg.

5) Personalized Federated Learning with Moreau Envelopes (**pFedMe**) (T Dinh et al., 2020), which aims to address statistical diversity among different sites. It uses Moreau envelopes as local sites' regularized loss functions, helping decouple the optimization process of the local model from the global model learning process. Thus, the global model can be utilized to optimize the local model.

3. Empirical Evaluation

3.1. Materials and Data Processing

3.1.1. Datasets

We employ a real fMRI dataset (called NYU) for model evaluation. This dataset consists of 50 patients diagnosed with autism spectrum disorder (ASD) and 50 healthy controls (HCs). All subjects are randomly sampled from the NYU site of ABIDE⁴. We utilize this dataset to explore the diagnostic capabilities of all introduced models, *i.e.*, classifying ASD patients from HCs. Moreover, to evaluate the effectiveness of federated learning strategies, we include two more sites from ABIDE, *i.e.*, UM and UCLA, to help train a global model and evaluate diagnostic performance in each site. The demographic characteristics of all studied subjects are shown in Table 2, while subject IDs are reported in *Supplementary Materials*.

3.1.2. Data Preprocessing

A standardized fMRI preprocessing pipeline based on Data Processing Assistant for Resting-State fMRI (DPARSF) (Yan and Zang, 2010) is utilized for preprocessing all fMRI scans, including discarding the first 10 volumes, slice timing correction, head motion estimation, bandpass

⁴http://fcon_1000.projects.nitrc.org/indi/abide

Table 2

Demographic characteristics of the studied subjects of three sites (*i.e.*, NYU, UM, and UCLA) from the public ABIDE cohort (Craddock et al., 2013). ASD: autism spectrum disorder; HC: healthy control; M/F: Male/Female; std: standard deviation.

Group	NYU		UM		UCLA	
	ASD	HC	ASD	HC	ASD	HC
Subject No.	50	50	40	40	30	30
Gender (M/F)	42/8	39/11	34/6	30/10	28/2	25/5
Age (mean \pm std)	12.39 \pm 5.51	15.12 \pm 6.58	13.55 \pm 2.32	14.46 \pm 2.89	12.86 \pm 2.45	13.09 \pm 2.06

Table 3

Results of machine learning models in ASD vs. HC classification on NYU. ASD: autism spectrum disorder; HC: healthy control.

Model	AUC (%)	Accuracy (%)	Balanced Accuracy (%)	F1-score (%)	Sensitivity (%)	Specificity (%)	Precision (%)
SVM	89.88 \pm 2.25	79.00 \pm 8.60	79.94 \pm 8.20	78.88 \pm 10.64	83.91 \pm 6.74	75.97 \pm 13.97	76.21 \pm 16.42
RF	85.68 \pm 8.46	75.00 \pm 12.25	75.83 \pm 12.26	73.77 \pm 11.26	70.83 \pm 19.36	80.83 \pm 13.33	81.33 \pm 11.62
XGBoost	83.92 \pm 7.45	72.00 \pm 10.30	72.76 \pm 10.28	72.23 \pm 11.24	76.95 \pm 16.36	68.57 \pm 9.93	69.81 \pm 11.56
KNN	77.35 \pm 10.64	63.00 \pm 9.80	63.57 \pm 5.07	71.38 \pm 9.44	96.35 \pm 4.64	30.80 \pm 8.54	57.79 \pm 12.55

filtering, regression of nuisance covariates, co-registration between T1-weighted images and mean functional images, and transformations from individual native space to the Montreal Neurological Institute (MNI) template space. In this work, we use the Automated Anatomical Labeling (AAL) atlas with $N = 116$ ROIs for brain ROI parcellation, resulting in regional mean fMRI time series for each subject.

3.2. Evaluation of Machine Learning Models

We first validate the performance of conventional machine learning models introduced in Section 2.4.1 based on fMRI data from NYU. Specifically, given the fMRI time series data, we first use Pearson’s correlation to construct a functional brain network for each subject. Then, we flatten the upper triangle elements of the network and convert them into a vectorized representation. For all experiments, we utilize PCA to reduce the feature dimension to 20, and we choose 5-fold cross-validation for model training. After inputting fMRI features and corresponding diagnostic labels into our toolbox, we can easily obtain classification results for each model, shown in Table 3. It can be seen from Table 3 that these machine learning models yield promising results in classifying ASD patients from HCs, indicating their effectiveness and efficacy. Additionally, our toolbox provides functionality for plotting the confusion matrix and AUC graph, enabling users to visualize prediction results. Fig. 7 presents these results for the conventional machine learning models included in ACTION.

3.3. Evaluation of Deep Learning Models

In the first group of experiments, we validate the performance of ten deep learning models for ASD diagnosis on fMRI from NYU using a 5-fold cross-validation strategy. All models are initialized using the pretrained deep learning models and finetuned on the training set of NYU, with classification results shown in Table 4. From Table 4, we can observe that these deep learning models achieve satisfactory performance in ASD identification.

In the second group of experiments, we evaluate the effectiveness of federated learning strategies introduced in

our toolbox. Here, we employ the pretrained GCN as the baseline model, based on which we apply different strategies. The classification results for ASD diagnosis of five federated learning strategies are reported in Table 5. Moreover, we include two non-federated learning methods (*i.e.*, Single and Mix) for comparison. Specifically, the “Single” method only uses data from a single site for model training and test via 5-fold cross-validation, without performing knowledge transfer/sharing among the individual sites. The “Mix” method uses all data pooled from all sites. The results of the “Single” method in “Average Results” are derived as follows. We first obtain prediction results for each site and then concatenate these results from all three sites. Then, with corresponding ground-truth labels, we can perform model prediction and obtain the results. A 5-fold cross-validation strategy is employed in these seven competing methods.

It can be seen from Table 5 that the federated learning models generally outperform the “Single” method. The underlying reason may be that federated learning enables capturing diverse fMRI features from multiple data sites, which can help enhance model generalization and thus yield better prediction results. In addition, these models also show superior classification results compared with the “Mix” method. The possible reason may be that federated learning enables multiple sites to train models collaboratively, which allows each site to leverage complementary knowledge from other sites, thus enhancing classification performance.

3.4. Limitation and Future Work

Several limitations need to be addressed in the future. *First*, current toolbox investigates fMRI data augmentation strategies from time series and graph perspectives. Benefiting from promising prospects of generative models in data augmentation, future work will explore innovative generative methods (*e.g.*, diffusion models (Yang et al., 2023a)) to enhance data diversity and scale. *Second*, the existing toolbox limits users to training deep learning models using only their local computing resources. In the future, we plan to develop a cloud computation platform, which empowers users with limited computation resources to engage in deep

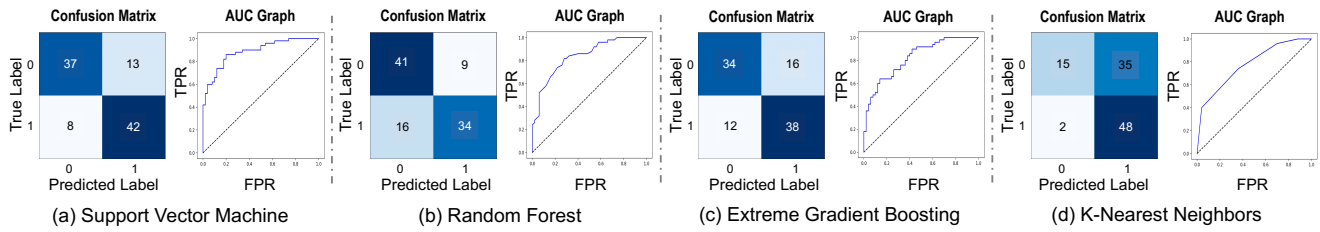


Figure 7: Demonstration of the confusion matrix and AUC graph generated by four conventional machine learning methods for ASD diagnosis on NYU. AUC: area under the receiver operating characteristic curve; TPR: true positive rate; FPR: false positive rate; 1: patients with autism spectrum disorder (ASD); 0: healthy controls.

Table 4

Results of deep learning models in ASD vs. HC classification on NYU. ASD: autism spectrum disorder; HC: healthy control.

Model	AUC (%)	Accuracy (%)	Balanced Accuracy (%)	F1-score (%)	Sensitivity (%)	Specificity (%)	Precision (%)
Transformer	76.00±14.36	60.00±16.96	63.13±15.91	67.49±12.85	83.16±15.32	43.09±36.34	60.68±23.02
GCN	74.61±11.33	59.00±14.32	62.69±11.74	58.99±6.57	61.03±25.02	64.36±43.53	73.00±27.75
GAT	77.87±10.96	67.00±9.75	68.53±10.89	65.54±12.98	66.12±17.60	70.94±24.31	69.56±20.30
GIN	72.17±12.56	61.00±12.94	64.45±12.09	64.21±7.04	70.32±18.85	58.58±37.38	67.23±24.61
GraphSAGE	72.12±17.57	66.00±13.87	67.37±13.02	62.10±26.94	72.02±35.84	62.72±29.00	71.56±22.84
BrainNetCNN	82.92±14.00	79.00±9.62	77.94±9.29	77.04±13.50	77.07±22.71	78.80±13.43	79.88±7.86
BrainGNN	87.09±3.98	75.00±8.66	75.56±11.16	69.15±20.50	65.85±27.43	85.27±12.10	79.57±13.37
STGCN	61.25±9.95	60.00±6.12	58.75±4.82	61.61±6.87	67.18±20.44	50.33±28.21	60.21±8.51
STAGIN	87.51±11.82	79.00±8.22	80.99±7.60	80.16±7.52	86.77±20.34	75.21±18.37	78.88±12.74
MGNN	78.16±5.70	73.00±7.58	72.95±7.57	73.18±10.71	77.72±8.92	68.18±7.78	69.92±14.48

learning fMRI analysis. *In addition*, although our toolbox offers a user-friendly interface with graphical controls and visualizations, it is constrained by compatibility with specific package versions. We intend to address this issue by creating a Docker container that encapsulates all necessary environments and dependencies in the future. *Lastly*, current work only supports the construction of AI-based models individually without leveraging multiple models that may capture complementary fMRI patterns. It is interesting to incorporate advanced ensemble learning algorithms (Yang et al., 2023b) into this toolbox to further boost its utility.

4. Conclusion

This paper introduces a Python-based cross-platform toolbox, called ACTION, for computer-aided functional MRI analysis. The ACTION consists of four components: *i.e.*, fMRI data augmentation, brain network construction, brain network feature extraction, and artificial intelligent model construction. It incorporates state-of-the-art fMRI data augmentation strategies and deep learning models. Moreover, federated learning strategies are embedded in our toolbox to help users implement their multisite fMRI studies without centralized data storage and computation. Experiments on three fMRI sites suggest the effectiveness and user-friendliness of ACTION. We hope our ACTION can benefit researchers in analyzing fMRI more efficiently.

Declarations of Interest

The authors declare that they have no known competing financial interests or personal relationships that could have appeared to influence the work reported in this paper.

Acknowledgement

Part of the data used in this work are from the ABIDE initiative, REST-meta-MDD project, and ADHD-200 Sample initiative. The investigators of ABIDE, REST-meta-MDD, and ADHD-200 provide the data but are not involved in data processing, analysis, toolbox development, and writing.

References

- Barrat, A., Barthelemy, M., Pastor-Satorras, R., Vespignani, A., 2004. The architecture of complex weighted networks. *Proceedings of the National Academy of Sciences* 101, 3747–3752.
- Bonach, P., 2007. Some unique properties of eigenvector centrality. *Social Networks* 29, 555–564.
- Breiman, L., 2001. Random forests. *Machine Learning* 45, 5–32.
- Brigham, E.O., 1988. *The fast Fourier transform and its applications*. Prentice-Hall, Inc.
- Chen, T., Guestrin, C., 2016. XGBoost: A scalable tree boosting system, in: *Proceedings of the 22nd ACM SIGKDD International Conference on Knowledge Discovery and Data Mining*, pp. 785–794.
- Chen, X., He, K., 2021. Exploring simple Siamese representation learning, in: *CVPR*, pp. 15750–15758.
- Cohen, I., Huang, Y., Chen, J., Benesty, J., Benesty, J., Chen, J., Huang, Y., Cohen, I., 2009. Pearson correlation coefficient. *Noise Reduction in Speech Processing*, 1–4.
- Craddock, C., Benhajali, Y., Chu, C., Chouinard, F., Evans, A., Jakab, A., Khundrakpam, B.S., Lewis, J.D., Li, Q., Milham, M., Yan, C., Bellec, P., 2013. The neuro bureau preprocessing initiative: Open sharing of preprocessed neuroimaging data and derivatives. *Frontiers in Neuroinformatics* 7, 27.
- Dai, Z., Lin, Q., Li, T., Wang, X., Yuan, H., Yu, X., He, Y., Wang, H., 2019. Disrupted structural and functional brain networks in Alzheimer’s disease. *Neurobiology of Aging* 75, 71–82.
- De La Fuente, A., Bing, N., Hoeschele, I., Mendes, P., 2004. Discovery of meaningful associations in genomic data using partial correlation coefficients. *Bioinformatics* 20, 3565–3574.
- Dvornek, N.C., Yang, D., Ventola, P., Duncan, J.S., 2018. Learning generalizable recurrent neural networks from small task-fMRI datasets, in:

Table 5

Results of federated learning models and baselines in ASD vs. HC classification on three sites (*i.e.*, NYU, UM, and UCLA). The average results across three sites are also provided. ASD: autism spectrum disorder; HC: healthy control.

Results on NYU Site	AUC (%)	Accuracy (%)	Balanced Accuracy (%)	F1-score (%)	Sensitivity (%)	Specificity (%)	Precision (%)
Single	65.6±11.0	65.0±11.4	65.0±11.4	70.5±8.1	84.0±16.0	46.0±28.7	60.9±11.3
FedAvg	75.2±9.1	69.0±10.2	69.0±10.2	68.0±9.9	66.0±9.4	72.0±13.2	70.2±12.1
FedProx	75.6±12.9	69.0±9.1	69.0±9.1	68.7±8.3	68.0±11.7	70.0±16.7	69.4±12.1
MOON	74.3±9.2	72.0±8.3	72.0±8.3	71.4±15.2	70.0±9.3	74.0±11.9	72.9±11.7
LGFedAvg	75.8±10.7	73.0±10.7	73.0±10.7	73.8±11.4	76.0±13.6	70.0±9.4	71.7±11.1
pFedMe	75.4±8.2	71.0±9.5	71.0±9.5	71.3±9.6	72.0±10.1	70.0±11.7	70.6±13.1
Results on UM Site	AUC (%)	Accuracy (%)	Balanced Accuracy (%)	F1-score (%)	Sensitivity (%)	Specificity (%)	Precision (%)
Single	73.4±19.0	61.7±6.7	61.7±6.7	41.0±17.7	26.7±26.7	96.7±6.7	88.9±8.0
FedAvg	54.1±12.6	56.7±6.2	56.7±6.2	31.6±19.1	20.0±25.5	93.3±8.2	75.0±27.4
FedProx	63.3±18.2	60.0±14.3	60.0±14.3	60.0±22.3	60.0±25.8	60.0±17.0	60.0±16.3
MOON	62.6±13.8	61.7±11.3	61.7±11.3	62.3±15.9	63.3±19.4	60.0±22.6	61.3±11.9
LGFedAvg	74.8±12.0	63.3±12.5	63.3±12.5	62.1±13.5	60.0±16.3	66.7±14.9	64.3±15.1
pFedMe	63.3±15.1	60.0±13.3	60.0±13.3	55.6±19.8	50.0±24.5	70.0±12.5	62.5±18.0
Results on UCLA Site	AUC (%)	Accuracy (%)	Balanced Accuracy (%)	F1-score (%)	Sensitivity (%)	Specificity (%)	Precision (%)
Single	64.3±14.2	63.7±12.1	63.7±12.1	72.9±7.3	97.5±30.0	30.0±23.2	58.2±8.8
FedAvg	69.1±17.8	63.8±12.1	63.8±12.1	54.0±15.8	42.5±14.2	85.0±12.2	73.9±9.8
FedProx	67.2±17.8	65.0±18.8	65.0±18.8	69.6±15.9	80.0±21.5	50.0±16.2	61.5±8.8
MOON	71.5±15.7	63.8±12.7	63.8±12.7	69.5±10.3	82.5±21.5	45.0±20.3	60.0±10.2
LGFedAvg	66.0±15.9	62.5±11.1	62.5±11.1	58.3±7.7	52.5±6.1	72.5±21.5	65.6±19.1
pFedMe	67.6±17.0	62.5±16.3	62.5±16.3	65.9±15.5	72.5±17.6	52.5±16.5	60.4±12.8
Average Results	AUC (%)	Accuracy (%)	Balanced Accuracy (%)	F1-score (%)	Sensitivity (%)	Specificity (%)	Precision (%)
Single	64.3±6.4	63.7±4.3	63.7±4.3	67.2±4.5	74.2±8.5	53.3±4.9	61.3±3.5
Mix	63.6±3.1	60.4±2.6	60.4±2.6	56.2±11.6	50.8±21.5	70.0±20.5	62.9±10.7
FedAvg	66.4±6.0	64.2±4.8	64.2±4.8	56.6±6.1	46.7±19.1	81.7±7.3	71.8±8.7
FedProx	69.7±7.3	65.4±9.4	65.4±9.4	66.9±8.1	70.0±7.5	60.8±15.0	64.1±9.8
MOON	70.8±9.4	66.7±9.6	66.7±9.6	68.5±9.0	72.5±11.0	60.8±11.1	64.9±8.4
LGFedAvg	71.9±8.6	67.1±8.3	67.1±8.3	66.1±7.4	64.2±8.5	70.0±12.2	68.1±8.9
pFedMe	69.8±7.6	65.4±8.2	65.4±8.2	65.8±8.1	66.7±11.4	64.2±11.4	65.0±8.4

- International Conference on Medical Image Computing and Computer-Assisted Intervention, Springer. pp. 329–337.
- Edde, M., Leroux, G., Altena, E., Chanraud, S., 2021. Functional brain connectivity changes across the human life span: From fetal development to old age. *Journal of Neuroscience Research* 99, 236–262.
- Fang, Y., Wang, M., Potter, G.G., Liu, M., 2023. Unsupervised cross-domain functional MRI adaptation for automated major depressive disorder identification. *Medical Image Analysis* 84, 102707.
- Fix, E., 1985. Discriminatory analysis: Nonparametric discrimination, consistency properties. volume 1. USAF School of Aviation Medicine.
- Fox, M.D., Raichle, M.E., 2007. Spontaneous fluctuations in brain activity observed with functional magnetic resonance imaging. *Nature Reviews Neuroscience* 8, 700–711.
- Freedman, D., Pisani, R., Purves, R., 2007. *Statistics (International Student Edition)*. Pisani, R. Purves, 4th edn. WW Norton & Company, New York.
- Freeman, L.C., et al., 2002. Centrality in social networks: Conceptual clarification. *Social Network: Critical Concepts in Sociology*. Londres: Routledge 1, 238–263.
- Gadgil, S., Zhao, Q., Pfefferbaum, A., Sullivan, E.V., Adeli, E., Pohl, K.M., 2020. Spatio-temporal graph convolution for resting-state fMRI analysis, in: *International Conference on Medical Image Computing and Computer Assisted Intervention*, Springer. pp. 528–538.
- Göttlich, M., Beyer, F., Krämer, U.M., 2015. BASCO: A toolbox for task-related functional connectivity. *Frontiers in Systems Neuroscience* 9, 126.
- Grotegerd, D., Redlich, R., Almeida, J.R., Riemenschneider, M., Kugel, H., Arolt, V., Dannlowski, U., 2014. MANIA—A pattern classification toolbox for neuroimaging data. *Neuroinformatics* 12, 471–486.
- Hamilton, W., Ying, Z., Leskovec, J., 2017. Inductive representation learning on large graphs. *Advances in Neural Information Processing Systems* 30.
- Hanke, M., Halchenko, Y.O., Sederberg, P.B., Hanson, S.J., Haxby, J.V., Pollmann, S., 2009. PyMVPA: A python toolbox for multivariate pattern analysis of fMRI data. *Neuroinformatics* 7, 37–53.
- Hearst, M.A., Dumais, S.T., Osuna, E., Platt, J., Scholkopf, B., 1998. Support vector machines. *IEEE Intelligent Systems and Their Applications* 13, 18–28.
- Hotelling, H., 1992. Relations between two sets of variates, in: *Breakthroughs in statistics: Methodology and distribution*. Springer, pp. 162–190.
- Hu, R., Peng, Z., Zhu, X., Gan, J., Zhu, Y., Ma, J., Wu, G., 2021. Multi-band brain network analysis for functional neuroimaging biomarker identification. *IEEE Transactions on Medical Imaging* 40, 3843–3855.
- Hyvärinen, A., Oja, E., 1997. A fast fixed-point algorithm for independent component analysis. *Neural Computation* 9, 1483–1492.
- Kaiser, M., 2011. A tutorial in connectome analysis: Topological and spatial features of brain networks. *NeuroImage* 57, 892–907.
- Kawahara, J., Brown, C.J., Miller, S.P., Booth, B.G., Chau, V., Grunau, R.E., Zwicker, J.G., Hamarneh, G., 2017. BrainNetCNN: Convolutional neural networks for brain networks; towards predicting neurodevelopment. *NeuroImage* 146, 1038–1049.
- Kim, B.H., Ye, J.C., 2020. Understanding graph isomorphism network for rs-fMRI functional connectivity analysis. *Frontiers in Neuroscience* , 630.
- Kim, B.H., Ye, J.C., Kim, J.J., 2021. Learning dynamic graph representation of brain connectome with spatio-temporal attention. *Advances in Neural Information Processing Systems* 34, 4314–4327.
- Kipf, T.N., Welling, M., 2016. Semi-supervised classification with graph convolutional networks. *arXiv preprint arXiv:1609.02907*.
- Kraskov, A., Stögbauer, H., Grassberger, P., 2004. Estimating mutual information. *Physical Review E* 69, 066138.
- Kruschwitz, J., List, D., Waller, L., Rubinov, M., Walter, H., 2015. GraphVar: A user-friendly toolbox for comprehensive graph analyses of functional brain connectivity. *Journal of Neuroscience Methods* 245, 107–115.
- Lanka, P., Rangaprakash, D., Gotoor, S.S.R., Dretsch, M.N., Katz, J.S., Denney Jr, T.S., Deshpande, G., 2020. MALINI (Machine Learning in NeuroImaging): A MATLAB toolbox for aiding clinical diagnostics using resting-state fMRI data. *Data in Brief* 29, 105213.
- Latora, V., Marchiori, M., 2001. Efficient behavior of small-world networks. *Physical Review Letters* 87, 198701.
- Le Guennec, A., Malinowski, S., Tavenard, R., 2016. Data augmentation for time series classification using convolutional neural networks, in: *ECML/PKDD Workshop on Advanced Analytics and Learning on Temporal Data*.

- Li, Q., He, B., Song, D., 2021a. Model-contrastive federated learning, in: Proceedings of the IEEE/CVF Conference on Computer Vision and Pattern Recognition, pp. 10713–10722.
- Li, T., Sahu, A.K., Zaheer, M., Sanjabi, M., Talwalkar, A., Smith, V., 2020. Federated optimization in heterogeneous networks. *Proceedings of Machine Learning and Systems* 2, 429–450.
- Li, X., Zhou, Y., Dvornik, N., Zhang, M., Gao, S., Zhuang, J., Scheinost, D., Staib, L.H., Ventola, P., Duncan, J.S., 2021b. BrainGNN: Interpretable brain graph neural network for fMRI analysis. *Medical Image Analysis* 74, 102233.
- Liang, P.P., Liu, T., Ziyin, L., Allen, N.B., Auerbach, R.P., Brent, D., Salakhutdinov, R., Morency, L.P., 2020. Think locally, act globally: Federated learning with local and global representations. *arXiv preprint arXiv:2001.01523*.
- Liao, W., Wu, G.R., Xu, Q., Ji, G.J., Zhang, Z., Zang, Y.F., Lu, G., 2014. DynamicBC: A matlab toolbox for dynamic brain connectome analysis. *Brain Connectivity* 4, 780–790.
- Lund, M.J., Alnæs, D., de Lange, A.M.G., Andreassen, O.A., Westlye, L.T., Kaufmann, T., 2022. Brain age prediction using fMRI network coupling in youths and associations with psychiatric symptoms. *NeuroImage: Clinical* 33, 102921.
- Ma, Q., Huang, B., Wang, J., Seger, C., Yang, W., Li, C., Wang, J., Feng, J., Weng, L., Jiang, W., et al., 2017. Altered modular organization of intrinsic brain functional networks in patients with Parkinson's disease. *Brain Imaging and Behavior* 11, 430–443.
- McMahan, B., Moore, E., Ramage, D., Hampson, S., y Arcas, B.A., 2017. Communication-efficient learning of deep networks from decentralized data, in: *Artificial Intelligence and Statistics*, PMLR. pp. 1273–1282.
- Meunier, D., Pascarella, A., Altukhov, D., Jas, M., Combrisson, E., Lajnef, T., Bertrand-Dubois, D., Hadid, V., Alamian, G., Alves, J., et al., 2020. NeuroPycon: An open-source python toolbox for fast multi-modal and reproducible brain connectivity pipelines. *NeuroImage* 219, 117020.
- Newman, M.E., 2002. Assortative mixing in networks. *Physical Review Letters* 89, 208701.
- Newman, M.E., 2003. The structure and function of complex networks. *SIAM Review* 45, 167–256.
- Newman, M.E., 2006. Modularity and community structure in networks. *Proceedings of the National Academy of Sciences* 103, 8577–8582.
- Paldino, M.J., Zhang, W., Chu, Z.D., Golriz, F., 2017. Metrics of brain network architecture capture the impact of disease in children with epilepsy. *NeuroImage: Clinical* 13, 201–208.
- Pei, S., Wang, C., Cao, S., Lv, Z., 2022. Data augmentation for fMRI-based functional connectivity and its application to cross-site ADHD classification. *IEEE Transactions on Instrumentation and Measurement* 72, 1–15.
- Recht, B., Fazel, M., Parrilo, P.A., 2010. Guaranteed minimum-rank solutions of linear matrix equations via nuclear norm minimization. *SIAM Review* 52, 471–501.
- Rubinov, M., Sporns, O., 2010. Complex network measures of brain connectivity: Uses and interpretations. *NeuroImage* 52, 1059–1069.
- Schrouff, J., Rosa, M.J., Rondina, J.M., Marquand, A.F., Chu, C., Ashburner, J., Phillips, C., Richiardi, J., Mourao-Miranda, J., 2013. PRoNTo: Pattern recognition for neuroimaging toolbox. *Neuroinformatics* 11, 319–337.
- Song, X.W., Dong, Z.Y., Long, X.Y., Li, S.F., Zuo, X.N., Zhu, C.Z., He, Y., Yan, C.G., Zang, Y.F., 2011. REST: A toolkit for resting-state functional magnetic resonance imaging data processing. *PLoS One* 6, e25031.
- T Dinh, C., Tran, N., Nguyen, J., 2020. Personalized federated learning with moreau envelopes. *Advances in Neural Information Processing Systems* 33, 21394–21405.
- Treder, M.S., 2020. MVPA-Light: A classification and regression toolbox for multi-dimensional data. *Frontiers in Neuroscience* 14, 491843.
- Vaswani, A., Shazeer, N., Parmar, N., Uszkoreit, J., Jones, L., Gomez, A.N., Kaiser, L., Polosukhin, I., 2017. Attention is all you need. *Advances in Neural Information Processing Systems* 30.
- Velivcković, P., Cucurull, G., Casanova, A., Romero, A., Lio, P., Bengio, Y., 2017. Graph Attention Networks. *arXiv preprint arXiv:1710.10903*.
- Waller, L., Brovkin, A., Dorfschmidt, L., Bzdok, D., Walter, H., Kruschwitz, J.D., 2018. GraphVar 2.0: A user-friendly toolbox for machine learning on functional connectivity measures. *Journal of Neuroscience Methods* 308, 21–33.
- Wang, H., Zhao, S., Dong, Q., Cui, Y., Chen, Y., Han, J., Xie, L., Liu, T., 2018. Recognizing brain states using deep sparse recurrent neural network. *IEEE Transactions on Medical Imaging* 38, 1058–1068.
- Wang, J., Wang, X., Xia, M., Liao, X., Evans, A., He, Y., 2015. GRETNA: A graph theoretical network analysis toolbox for imaging connectomics. *Frontiers in Human Neuroscience* 9, 386.
- Wang, Q., Wang, W., Fang, Y., Yap, P.T., Zhu, H., Li, H.J., Qiao, L., Liu, M., 2024. Leveraging brain modularity prior for interpretable representation learning of fMRI. *IEEE Transactions on Biomedical Engineering*.
- Wang, X., Chu, Y., Wang, Q., Cao, L., Qiao, L., Zhang, L., Liu, M., 2023. Unsupervised contrastive graph learning for resting-state functional MRI analysis and brain disorder detection. *Human Brain Mapping* 44, 5672–5692.
- Watts, D.J., Strogatz, S.H., 1998. Collective dynamics of ‘small-world’ networks. *Nature* 393, 440–442.
- Wen, Q., Sun, L., Yang, F., Song, X., Gao, J., Wang, X., Xu, H., 2021. Time series data augmentation for deep learning: A survey, pp. 4653–4660. doi:10.24963/ijcai.2021/631.
- Whitfield-Gabrieli, S., Nieto-Castanon, A., et al., 2012. Conn: A functional connectivity toolbox for correlated and anticorrelated brain networks. *Brain Connectivity* 2, 125–141.
- Wold, S., Esbensen, K., Geladi, P., 1987. Principal component analysis. *Chemometrics and Intelligent Laboratory Systems* 2, 37–52.
- Xiao, C., Ye, J., Esteves, R.M., Rong, C., 2016. Using spearman's correlation coefficients for exploratory data analysis on big dataset. *Concurrency and Computation: Practice and Experience* 28, 3866–3878.
- Xu, K., Liu, Y., Zhan, Y., Ren, J., Jiang, T., 2018. BRANT: A versatile and extendable resting-state fMRI toolkit. *Frontiers in Neuroinformatics* 12, 52.
- Xu, Z., Chang, X., Xu, F., Zhang, H., 2012. $L_{1/2}$ regularization: A thresholding representation theory and a fast solver. *IEEE Transactions on Neural Networks and Learning Systems* 23, 1013–1027.
- Yan, C., Zang, Y., 2010. DPARSF: A MATLAB toolbox for “pipeline” data analysis of resting-state fMRI. *Frontiers in Systems Neuroscience* 4, 1377.
- Yang, L., Zhang, Z., Song, Y., Hong, S., Xu, R., Zhao, Y., Zhang, W., Cui, B., Yang, M.H., 2023a. Diffusion models: A comprehensive survey of methods and applications. *ACM Computing Surveys* 56, 1–39.
- Yang, Y., Lv, H., Chen, N., 2023b. A survey on ensemble learning under the era of deep learning. *Artificial Intelligence Review* 56, 5545–5589.
- You, Y., Chen, T., Sui, Y., Chen, T., Wang, Z., Shen, Y., 2020. Graph contrastive learning with augmentations. *Advances in Neural Information Processing Systems* 33, 5812–5823.
- Zegura, E.W., Calvert, K.L., Bhattacharjee, S., 1996. How to model an internetwork, in: *Proceedings of IEEE INFOCOM'96. Conference on Computer Communications*, IEEE. pp. 594–602.
- Zhang, H., Chen, X., Shi, F., Li, G., Kim, M., Giannakopoulos, P., Haller, S., Shen, D., 2016. Topographical information-based high-order functional connectivity and its application in abnormality detection for mild cognitive impairment. *Journal of Alzheimer's Disease* 54, 1095–1112.
- Zhang, S., Chen, X., Shen, X., Ren, B., Yu, Z., Yang, H., Jiang, X., Shen, D., Zhou, Y., Zhang, X.Y., 2023. A-GCL: Adversarial graph contrastive learning for fMRI analysis to diagnose neurodevelopmental disorders. *Medical Image Analysis* 90, 102932.
- Zhou, Z., Chen, X., Zhang, Y., Hu, D., Qiao, L., Yu, R., Yap, P.T., Pan, G., Zhang, H., Shen, D., 2020. A toolbox for brain network construction and classification (BrainNetClass). *Human Brain Mapping* 41, 2808–2826.